LAWRENCE
LIVERMORE
NATIONAL
LABORATORY

LLNL-JRNL-674461

Study of a Mixed Dispersal Population Dynamics Model

M. Chugunova, B. Jadamba, C. Y. Kao, C. F. Klymko, E. Thomas, B. Zhao

July 10, 2015

The IMA Volumes in Mathematics and its Applications

Disclaimer

Study of a Mixed Dispersal Population Dynamics Model

Marina Chugunova, Baasansuren Jadamba, Chiu-Yen Kao, Christine Klymko, Evelyn Thomas, and Bingyu Zhao

Abstract In this paper, we consider a mixed dispersal model with periodic and Dirichlet boundary conditions and its corresponding linear eigenvalue problem. This model describes the time evolution of a population which disperses both locally and non-locally. We investigate how long time dynamics depend on the parameter values. Furthermore, we study the minimization of the principal eigenvalue under the constraints that the resource function is bounded from above and below, and with a fixed total integral. Biologically, this minimization problem is motivated by the question of determining the optimal spatial arrangement of favorable and unfavorable regions for the species to die out more slowly or survive more easily. Our numerical simulations indicate that the optimal favorable region tends to be a simply-connected domain. Numerous results are shown to demonstrate various scenarios of optimal favorable regions for periodic and Dirichlet boundary conditions.

Marina Chugunova
Department of Mathematics, Claremont Graduate University, Claremont, CA 91711, e-mail: marina.chugunova@cgu.edu
Baasansuren Jadamba
School of Mathematical Sciences, Rochester Institute of Technology, Rochester, NY 14623, e-mail: bxjsma@rit.edu
Chiu-Yen Kao
Department of Mathematical Sciences, Claremont McKenna College, Claremont, CA 91711, e-mail: ckao@cmc.edu
Christine Klymko
Center for Applied Scientific Computing, Lawrence Livermore National Laboratory, Livermore, CA 94550, e-mail: klymko1@llnl.gov
Evelyn Thomas
Department of Mathematics and Statistics, University of Maryland Baltimore County, Baltimore, MD 21250, e-mail: ekthomas@umbc.edu
Bingyu Zhao
Department of Applied Mathematics, Brown University, Providence, RI 02912, e-mail: bingyu_zhao@brown.edu

1 Introduction

To describe the dispersal of species, population dynamics models are commonly used. Random dispersal describes the movement of organisms between adjacent spatial locations [30, 6]. However, the movement of some organisms such as seeds of plants can occur between non-adjacent spatial locations and is thus non-local. In the recent years, there have been extensive studies on nonlocal models [7, 17, 10, 15, 14, 11, 13, 28, 21, 22, 12, 16, 29, 31, 1, 27, 2] and mixed models [18, 24, 32]. Here, we work on a mixed model which was proposed in [24] and study the time evolution problem and optimization of its corresponding eigenvalue problem under a heterogeneous environment.

The model which describes the species adopting both local and nonlocal dispersal is of the form

$$\frac{\partial u}{\partial t} = d\left[\tau\Delta u + (1-\tau)\mathscr{K}u\right] + f(x,u), \quad t>0, x\in\mathbb{R}^N \tag{1}$$

where $u(x,t)$ denotes the density of species at location x and time t, and the expression $\Delta = \Sigma_{i=1}^{N}\frac{\partial^2}{\partial x_i^2}$ is the Laplace operator in $\mathbb{R}^N$ accounting for random dispersal of species. The nonlocal operator $\mathscr{K}$ is defined by

$$(\mathscr{K}u)(x) := \int_{\mathbb{R}^N} k(|x-y|)\,u(y)\mathrm{d}y - u(x) \tag{2}$$

where $k = k(r)$ is a smooth and monotone decreasing function with compact support and $k(r)$ satisfies

$$\omega_N \int_0^\infty k(r) r^{N-1} dr = 1 \tag{3}$$

where ω_N denotes the area of the surface of the $N-$dimensional unit ball. Additionally, d is a positive constant which measures the total number of dispersal individuals per unit time, the constant $0<\tau\leq 1$ measures the fraction of individuals adopting random dispersal, and, if the logistic model is used, the reaction term is

$$f(x,u) = u(m(x)-u) \tag{4}$$

where $m(x)$ represents the resource function. In the biological applications, it is common to assume that $m(x)$ satisfies

$$-m_1 \leq m(x) \leq m_2 \text{ and } \int_\Omega m(x)\mathrm{d}x = M \tag{5}$$

where m_1 and m_2 are positive constants and the constant M could be positive or negative depending on whether the environment is friendly or hostile. This resource function $m(x)$ is positive in the favorable part of habitat and negative in unfavorable one. For the kernel function in (3), we use $k(r) = k^*(r/\delta)/\delta^N$ with

$$k^*(r) = \begin{cases} C_N \exp\left(\frac{1}{|r|^2-1}\right) & \text{for } |r| < 1 \\ 0 & \text{for } |r| \geq 1 \end{cases} \tag{6}$$

where C_N is chosen so that (3) is satisfied. $C_N \approx 2.2523$ in one dimension while $C_N \approx 2.1436$ in two dimensions.

In this paper, we consider the mixed dispersal model (1) on a bounded domain Ω with Dirichlet and periodic boundary conditions. The model (1) on Ω with Dirichlet boundary conditions is given by

$$\begin{cases} u_t = d\left[\tau\Delta u + (1-\tau)\mathscr{K}u\right] + u(m(x)-u) & \text{for } x \in \Omega, \\ u(x,t) = 0 & \text{for } x \in \partial\Omega. \end{cases} \tag{7}$$

One can view this model as the model on $\mathbb{R}^{\mathbb{N}}$ by a zero extension of $u(x,t)$ from Ω to $\mathbb{R}^{\mathbb{N}}\backslash\Omega$.

The model (1) with the periodic boundary conditions is given by

$$\begin{cases} u_t = d\left[\tau\Delta u + (1-\tau)\mathscr{K}u\right] + u(m(x)-u) & \text{for } x \in \mathbb{R}^N, \\ u(x,t) = u(x+p,t) & \text{for } x \in \mathbb{R}^N, \end{cases} \tag{8}$$

where $p = (p_1, p_2, ..., p_N)$ is a constant vector and the condition $u(x) = u(x+p)$ for $x \in \mathbb{R}^N$ is the so-called $p-$periodic function. One can view this as a periodic extension from a finite domain $\Omega = (0,p_1) \times (0,p_2) \times \cdots \times (0,p_N)$ to $\mathbb{R}^N$. When the periodic conditions are considered, $m(x)$ is assumed to be p-periodic as well.

In the early publications, the focus was on the local dispersal corresponding to $\tau = 1$ in the model (7). The long term dynamics were analyzed in terms of values of the diffusion parameter d on a bounded domain $\Omega \subset \mathbb{R}^{\mathbb{N}}$ with Dirichlet boundary conditions [4, 5]. It was found that whether $u = 0$ is a global attractor depends on the relationship of d and the principal positive eigenvalue Λ_1 (the smallest positive simple eigenvalue with a corresponding eigenfunction with no sign change) of the indefinite weight eigenvalue problem

$$-\Delta\psi = \Lambda m(x)\psi$$

where $m(x)$ satisfies $\text{mes}\{\Omega^+ : m(x) > 0\} \neq 0$ (favorable region), $\text{mes}\{\Omega^- : m(x) < 0\} \neq 0$ (unfavorable region), and $\int m(x) = M < 0$. Here $\text{mes}\{X\}$ denotes the Lebesgue measure of X. It was also shown in [4, 5] that the model (7) with $\tau = 1$ yields a unique positive steady state which is a global attractor for nonnegative nontrivial solutions, provided d is sufficiently small namely $d < 1/\Lambda_1$. On the contrary, the solution $u = 0$ is a global attractor for nonnegative solutions if $d > 1/\Lambda_1$, so that the population tends to extinction.

This motivated studies on the minimization of the principal positive eigenvalue in terms of spatial heterogeneity of the resource $m(x)$, which allows species with larger dispersal rate d to survive. In [25, 20], the minimization of the principal eigenvalue was studied with Dirichlet, Neumann, and Robin boundary conditions. The optimal arrangement of $m(x)$ for Dirichlet boundary conditions prefers Ω^+ be a simply connected region away from the boundary on the convex domain. However, for

Neumann boundary conditions, Ω^+ remains a simply connected domain and leans toward to the part of boundaries with high curvature. For Robin boundary conditions $\frac{\partial u}{\partial n} + \beta u = 0$, there exists a threshold β^* at which a transition from a Dirichlet like scenario to Neumann like one occurs.

In [7], the model (1) with $\tau = 0$ and without the reaction term $f(x,u)$ was analyzed for long time behavior. The authors proved that similar to the heat equation, the solution exponentially converges to zero for Dirichlet boundary conditions and exponentially converges to the mean value of the initial condition for Neumann conditions. In [31], proofs of the existence and uniqueness of positive solutions for the nonlocal dispersal equation were obtained by the monotone iteration method. A recent result on the optimal distribution of resources when the total resource was fixed was obtained in [1]. The authors proved that the optimal $m(x)$ is of bang-bang type for the model (1) with $\tau = 0$ and a uniform kernel on a bounded domain $\Omega \subset \mathbb{R}$.

The stability of the equilibrium solution $u = 0$ of (7) and (8) depends on the sign of the principal eigenvalue of the corresponding linear eigenvalue problem

$$\mathscr{L}\phi \equiv -d\left[\tau\Delta\phi + (1-\tau)\,\mathscr{K}\phi\right] - m(x)\phi = \lambda\phi\ . \tag{9}$$

with the corresponding boundary conditions. It was shown in [24] that the principal eigenvalue can be expressed in a variational formulation

$$\lambda_p = \inf_{0\neq v\in\mathscr{H}^1(\Omega)} \frac{\int_{\Omega=(0,p_1)\times(0,p_2)\times\cdots\times(0,p_N)} v\mathscr{L}v\mathrm{d}x}{\int_{\Omega=(0,p_1)\times(0,p_2)\times\cdots\times(0,p_N)} v^2\mathrm{d}x} \tag{10}$$

for periodic boundary conditions and

$$\lambda_D = \inf_{0\neq v\in\mathscr{H}_0^1(\Omega)} \frac{\int_\Omega v\mathscr{L}v\mathrm{d}x}{\int_\Omega v^2\mathrm{d}x} \tag{11}$$

for Dirichlet boundary conditions.

When the principal eigenvalue is positive, $u = 0$ is a stable equilibrium and the species cannot invade from a low initial population. When the principal eigenvalue is negative, $u = 0$ is unstable and the species can invade from a low initial population. The interesting question is how the spatial heterogeneity of the resource which is represented by $m(x)$ can affect the principal eigenvalue.

Thus, we will study the optimization problem which looks for the minimal eigenvalue

$$\lambda_p^* = \min_{m(x)} \lambda_p \text{ and } \lambda_D^* = \min_{m(x)} \lambda_D, \tag{12}$$

when the resource function $m(x)$ is a bang-bang function subject to

$$m = -m_1 \text{ or } m_2 \text{ a.e. and } \int_\Omega m(x)\mathrm{d}x = M\ . \tag{13}$$

The rest of this paper is organized as follows. Sect. 2 is devoted to the analytic study of the mixed model with Dirichlet boundary conditions. In Sect. 3, we present nu-

merical approaches to solve time-dependent equations (7) and (8). We also study the corresponding linearized eigenvalue problem (9) and show how the eigenvalue varies with respect to diffusion coefficients d and τ. Furthermore, we use a rearrangement algorithm to find the optimal configuration of $m(x)$ in (12) which minimizes the principal eigenvalue so that the species will die out more slowly or survive more easily. Conclusions and future work are discussed in Sect. 5.

2 Analytical Results

In [24], the time evolution problem with periodic boundary conditions (8) was studied and the solution is nonnegative preserving (i.e. if the initial data $u(x,0)$ is nonnegative, the solution $u(x,t)$ remains nonnegative at all later times t.) For any value of the parameter $\delta \neq 0$ the integral operator $\mathscr{K}$ is of Hilbert-Schmidt type (that implies it is continuous and compact). $\mathscr{K}$ is a self-adjoint operator $L^2(\Omega) \to L^2(\Omega)$ [24].

In the following, we will focus on the proofs for the properties of mixed dispersal model with Dirichlet boundary conditions.

Theorem 1 *There exists a constant D^*, such that if the diffusion coefficient $d > D^*$, no positive stationary states of (1) exist.*

Proof. Let us first estimate the integration involving $\mathscr{K}$:

$$\begin{aligned}
\int_\Omega u(\mathscr{K}u)\,\mathrm{d}x &= \int_\Omega\int_\Omega u(x)k(|x-y|)u(y)\mathrm{d}y\mathrm{d}x - \int_\Omega u^2(x)\mathrm{d}x \\
&= \int_\Omega\int_\Omega u(x)k(|x-y|)u(y)\mathrm{d}y\mathrm{d}x - \int_\Omega k(|x-y|)\mathrm{d}y\int_\Omega u^2(x)\mathrm{d}x \\
&= \int_\Omega\int_\Omega u(x)\left[k(|x-y|)\left(u(y)-u(x)\right)\right]\mathrm{d}y\mathrm{d}x \\
&= \frac{1}{2}\int_\Omega\int_\Omega u(x)\left[k(|x-y|)\left(u(y)-u(x)\right)\right]\mathrm{d}y\mathrm{d}x \\
&+ \frac{1}{2}\int_\Omega\int_\Omega u(y)\left[k(|y-x|)\left(u(x)-u(y)\right)\right]\mathrm{d}x\mathrm{d}y \\
&= -\frac{1}{2}\int_\Omega\int_\Omega\left[k(|x-y|)\left(u(y)-u(x)\right)^2\right]\mathrm{d}y\mathrm{d}x \\
&\leq 0\,. \qquad (14)
\end{aligned}$$

Let $u(x)$ be a nonnegative stationary solution of (7). Then $u(x)$ satisfies

$$\tau\Delta u = -\frac{1}{d}u(m(x)-u) + (\tau-1)\mathscr{K}u$$

Multiplying the equation by u and integrating over the domain Ω, we obtain

$$\tau\int_\Omega u\Delta u\mathrm{d}x = -\frac{1}{d}\int_\Omega u^2(m(x)-u)\mathrm{d}x + (\tau-1)\int_\Omega u(\mathscr{K}u)\,\mathrm{d}x\,.$$

Integrating by parts and using the Dirichlet boundary conditions, we obtain

$$\tau \int_\Omega |\nabla u|^2 \mathrm{d}x = \frac{1}{d}\int_\Omega u^2(m(x)-u)\mathrm{d}x + (1-\tau)\int_\Omega u\,(\mathscr{K}u)\,\mathrm{d}x$$
$$\leq \frac{1}{d}\int_\Omega u^2 m(x)\mathrm{d}x \leq \frac{m_2}{d}\int_\Omega u^2 \mathrm{d}x\,.$$

Applying the Poincare inequality on the right hand side term, we obtain

$$\tau \int_\Omega |\nabla u|^2 \mathrm{d}x \leq c_\Omega \frac{m_2}{d}\int_\Omega |\nabla u|^2 \mathrm{d}x\,.$$

where c_Ω is a constant that depends on Ω. In one dimension, $c_\Omega = \frac{|\Omega|^2}{\pi^2}$. Thus

$$(d\tau - c_\Omega m_2)\int_\Omega |\nabla u|^2 \mathrm{d}x \leq 0$$

If

$$d \geq \frac{m_2 c_\Omega}{\tau} =: D^*, \tag{15}$$

it implies that we must have $u \equiv 0$. □

Theorem 2 *If $d > D^*$, then $||u||_1$ decays exponentially.*

Proof. Let us define the energy function $E(t) = \frac{1}{2}\int_\Omega u^2(x,t)\mathrm{d}x$. The rate of change of energy is

$$E'(t) = \int_\Omega u u_t \mathrm{d}x$$
$$= d\left(\tau\int_\Omega u\Delta u \mathrm{d}x + (1-\tau)u\,(\mathscr{K}u)\,\mathrm{d}x\right) + \int_\Omega m u^2 \mathrm{d}x - \int_\Omega u^3 \mathrm{d}x\,.$$

Dropping the last term due to the positivity preserving of the solution [24, 29], applying the kernel estimation (14) on the second term, and applying the Poincare inequality on the third term, we obtain

$$E'(t) \leq [-d\tau + m_2 c_\Omega]\int_\Omega |\nabla u|^2 \mathrm{d}x\,.$$

Denote $D := [-d\tau + m_2 c_\Omega]$. Note that $d > D^*$ implies that $D < 0$. Applying Poincare inequality again, we then have

$$E'(t) \leq D\int_\Omega |\nabla u|^2 \leq \frac{D}{c_\Omega}\int_\Omega u^2 \mathrm{d}x\,.$$

By using Grönwall's inequality, now we have

$$E(t) \leq E_0 \exp\left(\frac{2D}{c_\Omega}t\right)\,.$$

As a result we now have the decay rate estimation of 1-norm of $u(x,t)$:

$$\int_\Omega |u|\mathrm{d}x \le |\Omega|^{1/2}\left(\int_\Omega u^2\mathrm{d}x\right)^{1/2} = 2^{1/2}|\Omega|^{1/2}E^{1/2}(t)$$
$$\le (2|\Omega|E_0)^{1/2}\exp\left(\frac{D}{c_\Omega}t\right).$$

□

Theorem 3 *If $d < D^*, ||u||_1$ is bounded from above.*

Proof. Multiplying equation (7) by u and integrating over the domain Ω, we obtain

$$\int_\Omega u^3\mathrm{d}x = -d\tau\int_\Omega |\nabla u|^2\mathrm{d}x + d(1-\tau)\int_\Omega u\,(\mathscr{K}u)\,\mathrm{d}x + \int_\Omega m(x)u^2\mathrm{d}x$$

which implies that

$$||u||_3^3 = \int_\Omega u^3\mathrm{d}x \le \left(m_2 - \frac{d\tau}{c_\Omega}\right)\int_\Omega u^2\mathrm{d}x\,.$$

By using $||u^2||_{3/2} = ||u||_3^2$, we have

$$\int_\Omega u^2\mathrm{d}x \le \left(\int_\Omega \left(u^2\right)^{3/2}\mathrm{d}x\right)^{3/2}|\Omega|^{1/3} \le ||u||_3^2|\Omega|^{1/3}\,.$$

Thus,

$$||u||_3 \le \left(m_2 - \frac{d\tau}{c_\Omega}\right)|\Omega|^{1/3}\,.$$

We then have

$$||u||_1 = \int_\Omega u\mathrm{d}x \le \left(\int_\Omega u^3\mathrm{d}x\right)^{1/3}|\Omega|^{2/3}\,.$$
$$\le \left(m_2 - \frac{d\tau}{c_\Omega}\right)^{1/3}|\Omega|^{7/9}\,.$$

□

Note that the upper bound derived here is a decreasing function in d.

Theorem 4 *If $d > D^*$, the principal eigenvalue is positive if exists.*

Proof. Denote the normalized eigenfunction, i.e. $\int_\Omega \phi^2\mathrm{d}x = 1$, which corresponds to λ_D by ϕ, thus

$$\begin{aligned}\lambda_D &= -\int_\Omega \phi\left\{d\left[\tau\Delta\phi+(1-\tau)\mathscr{K}\phi\right]+m\phi\right\}\mathrm{d}x\\ &= \int_\Omega d\left[\tau|\nabla\phi|^2-(1-\tau)\phi\left(\mathscr{K}\phi\right)\right]-m\phi^2\mathrm{d}x\\ &\geq d\left[\frac{\tau}{c_\Omega}-\frac{m_2}{d}\right]\int_\Omega\phi^2\mathrm{d}x = d\left[\frac{\tau}{c_\Omega}-\frac{m_2}{d}\right].\end{aligned}$$

Thus if $d > D^*$ defined in (15), we have $\lambda_D > 0$. □

Theorem 5 *Let $\lambda_D(d_1)$ and $\lambda_D(d_2)$ be the corresponding principal eigenvalues for $d = d_1$ and $d = d_2$. If $d_1 > d_2$, then $\lambda_D(d_1) > \lambda_D(d_2)$.*

Proof. Denote the normalized eigenfunction which corresponds to $\lambda_D(d_1)$ by ϕ, thus

$$-\left\{d_1\left[\tau\Delta\phi+(1-\tau)\mathscr{K}\phi\right]+m\phi\right\} = \lambda_D(d_1)\phi\,. \tag{16}$$

Since ϕ is not necessarily the eigenfunction which corresponds to $\lambda_D(d_2)$, we have

$$-\int_\Omega\left\{d_2\left[\tau\Delta\phi+(1-\tau)\mathscr{K}\phi\right]+m\phi\right\}\phi\mathrm{d}x \geq \lambda_D(d_2)\,. \tag{17}$$

Multiplying (16) by ϕ, integrating by parts, and subtracting (17), we have

$$\lambda_D(d_1)-\lambda_D(d_2) \geq (d_1-d_2)\left[\tau\int|\nabla\phi|^2\mathrm{d}x-(1-\tau)\int\phi\left(\mathscr{K}\phi\right)\mathrm{d}x\right] > 0\,.$$

□

Theorem 6 *Let $\lambda_D(\tau_1)$ and $\lambda_D(\tau_2)$ be the corresponding principal eigenvalues for $\tau = \tau_1$ and $\tau = \tau_2$. For any given Ω with Poincare constant $c_\Omega < 1$, if $\tau_1 > \tau_2$, then $\lambda_D(\tau_1) > \lambda_D(\tau_2)$.*

Proof. Denote the normalized eigenfunction which corresponds to $\lambda_D(\tau_1)$ by ϕ, thus

$$-\left\{d\left[\tau_1\Delta\phi+(1-\tau_1)\mathscr{K}\phi\right]+m\phi\right\} = \lambda_D(\tau_1)\phi\,. \tag{18}$$

Since ϕ is not necessary the eigenfunction which corresponds to $\lambda_D(\tau_2)$, we have

$$-\int_\Omega\left\{d\left[\tau_2\Delta\phi+(1-\tau_2)\mathscr{K}\phi\right]+m\phi\right\}\phi\mathrm{d}x \geq \lambda_D(\tau_2)\,. \tag{19}$$

Multiplying (18) by ϕ, integrating by parts, and subtracting (19), we have

$$\begin{aligned}\lambda_D(\tau_1)-\lambda_D(\tau_2) &\geq d(\tau_1-\tau_2)\left[\int|\nabla\phi|^2\mathrm{d}x+\int\phi\left(\mathscr{K}\phi\right)\mathrm{d}x\right]\\ &\geq d(\tau_1-\tau_2)\left[\frac{1}{c_\Omega}\int\phi^2\mathrm{d}x-\int\phi^2\mathrm{d}x\right]\\ &\geq d(\tau_1-\tau_2)\left[\frac{1}{c_\Omega}-1\right]\int\phi^2\mathrm{d}x = d(\tau_1-\tau_2)\left[\frac{1}{c_\Omega}-1\right].\end{aligned}$$

If $c_\Omega < 1$, we have $\lambda_D(\tau_1) > \lambda_D(\tau_2)$. □

Theorem 7 *Let $m(x)$ be any given function satisfying (5) and $\bar{m}(\phi)$ be the bang-bang function satisfying (13) for the normalized eigenfunction $\phi(x)$ of $m(x)$, i.e. $\bar{m}(\phi) = m_2\chi_{E_\alpha} - m_1\chi_{E_\Omega\setminus\alpha}$ where $E_\alpha(\phi) = \{x \in \Omega : \phi^2(x) > \alpha\}$ and α is chosen so that $|E_\alpha|m_2 - |\Omega\setminus E_\alpha|m_1 = M$ holds. (In case $\phi = 0$ on a set of positive measure, it is also possible to choose such a bang-bang function. See [4]). Then, the principal eigenvalue satisfies*

$$\lambda_D(m) \geq \lambda_D(\bar{m}).$$

Proof. For any given eigenfunction ψ,

$$\begin{aligned}\int_\Omega (\bar{m}(\psi) - m)\,\psi^2 \mathrm{d}x &= \int_{E_\alpha} (m_2 - m)\,\psi^2 \mathrm{d}x + \int_{\Omega\setminus E_\alpha} (-m_1 - m)\,\psi^2 \mathrm{d}x \\ &\geq \alpha \int_{E_\alpha} (m_2 - m)\,\mathrm{d}x - \alpha \int_{\Omega\setminus E_\alpha} (m_1 + m)\,\mathrm{d}x \\ &= \alpha \int_{E_\alpha} (\bar{m} - m)\,\mathrm{d}x = 0,\end{aligned}$$

we obtain

$$\begin{aligned}\lambda_D(\bar{m}) &= \inf_{0\neq v\in H_0^1, ||v||_2=1} \int_\Omega -d\left[-\tau|\nabla v|^2 + (1-\tau)\,v(\mathscr{K}v)\right] - \bar{m}v^2 \mathrm{d}x \\ &\leq \int_\Omega -d\left[-\tau|\nabla\phi|^2 + (1-\tau)\,\phi(\mathscr{K}\phi)\right] - \bar{m}\phi^2 \mathrm{d}x \\ &\leq \int_\Omega -d\left[-\tau|\nabla\phi|^2 + (1-\tau)\,\phi(\mathscr{K}\phi)\right] - m(x)\phi^2 \mathrm{d}x \\ &= \lambda_D(m(x))\end{aligned}$$

where ϕ is the normalized eigenfunction corresponds to $m(x)$. The proof for $\lambda_p(\bar{m}) \leq \lambda_p(m)$ follows the same arguments. □

Here, we prove a theorem which is related to our rearrangement algorithm to find the optimal configuration of the resource function $m(x)$. Given a function $m(x)$ defined in Ω and satisfying (5), we say that $m_0(x)$ belongs to the class of rearrangements $\mathscr{R} = \mathscr{R}(m(x))$ if

$$\mathrm{mes}\{x \in \Omega : m_0(x) \geq \beta\} = \mathrm{mes}\{x \in \Omega : m(x) \geq \beta\}, \quad \forall \beta \geq 0\,.$$

Theorem 8 *Let $m_0(x)$ belongs to the class of rearrangements $\mathscr{R}(m(x))$. Denote by $\phi(x)$ and $\phi_0(x)$ the corresponding normalized eigenfunctions of resource functions $m(x)$ and $m_0(x)$, respectively. If*

$$\int_\Omega m_0\phi^2 \mathrm{d}x \geq \int_\Omega m\phi^2 \mathrm{d}x, \tag{20}$$

then $\lambda_D(m_0) \leq \lambda_D(m)$. Similarly, $\lambda_p(m_0) \leq \lambda_p(m)$.

Proof. By the definition of the principal eigenvalue, we have

$$\begin{aligned}\lambda_D(m_0(x)) &= \int_\Omega -d\left[-\tau|\nabla\phi_0|^2+(1-\tau)\,\phi_0(\mathscr{K}\phi_0)\right]-m_0(x)\phi_0^2\mathrm{d}x\\ &\le \int_\Omega -d\left[-\tau|\nabla\phi|^2+(1-\tau)\,\phi(\mathscr{K}\phi)\right]-m_0(x)\phi^2\mathrm{d}x\\ &\le \int_\Omega -d\left[-\tau|\nabla\phi|^2+(1-\tau)\,\phi(\mathscr{K}\phi)\right]-m(x)\phi^2\mathrm{d}x\\ &= \lambda_D(m(x))\,.\end{aligned}$$

The proof for $\lambda_p(m_0)\le\lambda_p(m)$ follows the same arguments. □

This result allows one to find a new configuration $m_0(x)$ satisfying (13) with a smaller eigenvalue for any given $m(x)$ satisfying (13). It is well known that $\sup_{m(x)}\int_\Omega m(x)\phi^2\mathrm{d}x$ is obtained when $m(x)$ is arranged to be a monotone increasing function in ϕ^2 [19] which means that the optimal choice is $\bar{m}(\phi)=m_2\chi_{E_\alpha}-m_1\chi_{E_\Omega\setminus\alpha}$ where $E_\alpha(\phi)=\left\{x\in\Omega:\phi^2(x)>\alpha\right\}$ and α is chosen so that $|E_\alpha|m_2-|\Omega\setminus E_\alpha|m_1=M$ holds.

3 Numerical Implementation

In this section, we discuss the numerical approaches to the mixed dispersal model with both Dirichlet and periodic boundary conditions. We solve the linearized eigenvalue problem (9) and time evolution problems (7) and (8), as well as the optimization problem which determines the optimal arrangement of the resources. For simplicity, we use finite difference approaches on one-dimensional interval and two-dimensional rectangular domains and use a finite element approach on general domains such as dumbbell shapes with Dirichlet boundary conditions.

3.1 Finite difference method

For one-dimensional finite difference approach, we use the method proposed in [24]. The model (1) in one dimensional interval $I=[0,L]$ is described by

$$u_t=d\left[\tau u_{xx}+(1-\tau)\left(\frac{1}{\delta}\int_I k^*\left(\frac{x-y}{\delta}\right)u(y)\mathrm{d}y-u(x)\right)\right]+u(m(x)-u), \quad (21)$$

with k^* defined in (6). The corresponding eigenvalue problem is

$$-d\left[\tau u_{xx}+(1-\tau)\left(\frac{1}{\delta}\int_I k^*\left(\frac{x-y}{\delta}\right)u(y)\mathrm{d}y-u(x)\right)\right]-m(x)u=\lambda u\,. \quad (22)$$

We discretize the domain by using a uniform mesh: $x_i=ih$ for $i=0,1,2,...,N$, with the mesh size $h=L/N$. Denote by u_i the numerical approximation of $u(x_i)$. For

Dirichlet boundary conditions, zero values are assigned to u_0 and u_N. We seek for the solution $\mathbf{U} = (u_1, u_2, ..., u_{N-1})^T$. For periodic boundary conditions, we have $u_0 = u_N$ and seek for the solution $\mathbf{U} = (u_1, ..., u_N)^T$. The local dispersal term u_{xx} is approximated by a second order central difference scheme and the nonlocal dispersal term involving integration is approximated by the trapezoidal method. The discretization of (21) leads to a system of ordinary differential equations. With given initial values of $\mathbf{U}$, we use forward Euler method to compute the solution at any later time under the stability restriction on the time stepsize. The discretization of (22) leads to a discrete eigenvalue problem and the principal eigenvalue can be easily computed using Arnoldi's method.

It is very straight forward to extend this method to solve (7) and (8) in two dimensions on a rectangular domain $[0, L_x] \times [0, L_y]$. We discretize the domain by using a mesh: $(x_i, y_j) = (ih_x, jh_y)$ for $i = 0, 1, 2, ..., N_x$ and $j = 0, 1, 2, ..., N_y$, with $h_x = L_x/N_x$ and $h_y = L_y/N_y$. Denote $u_{i,j}$ the numerical approximation of $u(x_i, y_j)$. Boundary conditions are enforced in the similar way in one dimension. The local dispersal term Δu is approximated by the five-point difference scheme

$$\Delta u(x_i, y_j) \approx \frac{u_{i+1,j} - 2u_{i,j} + u_{i-1,j}}{h_x^2} + \frac{u_{i,j+1} - 2u_{i,j} + u_{i,j-1}}{h_y^2}$$

and the nonlocal dispersal term involving integration of the kernel term

$$\int_0^{L_x} \int_0^{L_y} k(|(x,y) - (\tilde{x}, \tilde{y})|) u(\tilde{x}, \tilde{y}) d\tilde{x} d\tilde{y}$$

is done with a composite trapezoidal rule in two dimensions

$$\sum\sum k_{i,j,\tilde{i},\tilde{j}} w_{\tilde{i},\tilde{j}} u_{\tilde{i},\tilde{j}}$$

where $k_{i,j,\tilde{i},\tilde{j}}$ is $k(|(x_i, y_j) - (\tilde{x_i}, \tilde{y_j})|)$ and $w_{\tilde{i},\tilde{j}}$ are weights of composite trapezoidal rule. The discretization of (7) and (8) again leads to a system of ordinary differential equations while the discretization of (9) leads to a discrete eigenvalue problem.

3.2 Finite element method

On irregular domains, we use a finite element method to solve (9) with Dirichlet boundary conditions . We use bilinear elements on quadrilaterals for the eigenfunction, and the function $m(x)$ is represented by piecewise constants on the quadrilaterals. The discrete eigenvalue problem

$$PU = \lambda QU \tag{23}$$

where U is a solution vector with entries U_j $(j = 1, \ldots, n)$, P is the matrix resulting from the differential operator, integral operator, and the resource function term, and

Algorithm 1 A rearrangement algorithm to minimize the principal eigenvalue

Give an initial guess for $m(x)$ and compute the area of favorable region $|\Omega_+|$.
Repeat 1-3 until $m(x)$ does not change any more

1. Solve the eigenvalue problem (9) with Dirichlet or periodic boundary conditions by the finite difference method described in 3.1 or the finite element method described in 3.2.
2. Sort the value of ϕ^2 at the discrete points in the descending order and compute the threshold α such that $|\{x|\phi(x)^2 > \alpha\}| = |\Omega_+|$.
3. If $\phi(x)^2 >= \alpha$, assign $m(x) = m_2$. Otherwise, assign $m(x) = -m_1$.

Q is the mass matrix, is solved by using Arnoldi's algorithm. We use the deal.II finite element library [3] to do our computations.

3.3 Optimization approach based on a rearrangement algorithm

For finding the minimal principal eigenvalue in (12) subject to (13), we adopt the rearrangement algorithm proposed in [26]. Given an initial configuration of $m(x)$ which is bounded from below by $-m_1$ and bounded from above by m_2, one can calculate the area for the favorable region Ω_+. In the finite difference calculation, this is done by counting the number of the mesh points which have the value $m = m_2$ and multiplying by h in one dimension and by $h_x h_y$ in two dimensions. In the finite element approach, this is done by calculating the total area of the elements which have the value $m = m_2$. Next, using the rearrangement approach, we iterate $m(x)$ until the optimal configuration is reached. In each iteration, m_2 is assigned to the location where square values of magnitude of the eigenfunction is above the critical threshold α which is chosen when $|\{x|\phi(x)^2 > \alpha\}| = |\Omega_+|$ is satisfied. The algorithm is summarized in Algorithm 1. The stopping criterion is when two successive $m(x)$ are identically the same. If the algorithm stops at $n-$th iteration, it means that the optimal configuration is achieved at $(n-1)-$th iteration.

4 Numerical Results

In this section, we study how the principal eigenvalue changes for different values of coefficients d and τ, for both Dirichlet and periodic boundary conditions. Results from computations on square and rectangular domains in one and two dimensions are presented. We also present results of simulations on a general shaped domain in two dimensions.

4.1 One-Dimensional Results

We first study how the principal eigenvalue of Eq. (22) in the interval $[0,1]$ varies with respect to different values of coefficients, d and τ. In our experiments, we use mesh size $N = 400$ for periodic boundary conditions and $N = 1600$ for Dirichlet boundary conditions to guarantee at least two significant digits of accuracy for the principal eigenvalue. Given $m(x) = \chi_{[0.4,0.6]} - \chi_{[0,0.4)\cup(0.6,1]}$, we compute the principal eigenvalue for d ranging from 0 to 0.1 with $\tau = 0, 0.5$, and 1. In Figs. 1(a) and 1(b), we see that the principal eigenvalue becomes negative when the total diffusion coefficient d is relatively small in both periodic and Dirichlet cases. Furthermore, the principal eigenvalue becomes smaller as τ decreases. In Figs. 2(a) and 2(b), the change of λ_p and λ_D are shown with respect to τ ranging from 0 to 1 when $d = 0.01, 0.05, 0.1$, and 1. In both periodic and Dirichlet cases, we see that λ_p and λ_D become negative when τ is relatively small which means the species adopted more nonlocal diffusion. Furthermore, λ_p and λ_D are both monotone increasing functions in d with the current choice of parameters.

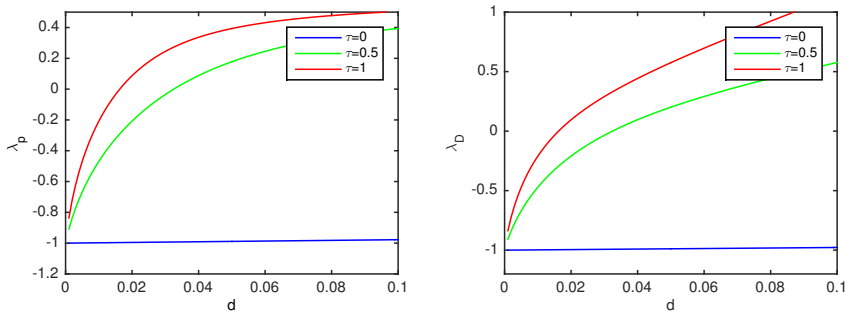

(a) (b)

Fig. 1 (a) λ_p versus d (b) λ_D versus d for $\tau = 0, 0.5$, and 1 with $\delta = 0.15$

For time evolution problems (7) and (8), we study the long term behavior of the solution. When the diffusion coefficient d is big enough, for example see Fig. 3 with $d = 2$, the whole population dies out as time goes to infinity. In Figs. 3(a) and 3(b), we plot the logarithm of the L_1 norm of u for both periodic and Dirichlet boundary conditions, upon which we also perform linear fitting, shown in Figs. 3(c) and 3(d). We can see that $||u||_{L_1}$ decays exponentially for both boundary conditions, which is consistent with our analytical result in Theorem 2. On the other hand, for small total diffusion d, the solution will finally reach a positive steady state for both periodic and Dirichlet boundary conditions, as illustrated in Fig. 4 when $d = 0.02$, where we plot the final configuration of u after time long enough to show the positive steady state.

Finally, we determine the optimal arrangement of $m(x)$ in an interval by using the rearrangement approach. It turns out that for both periodic and Dirichlet boundary

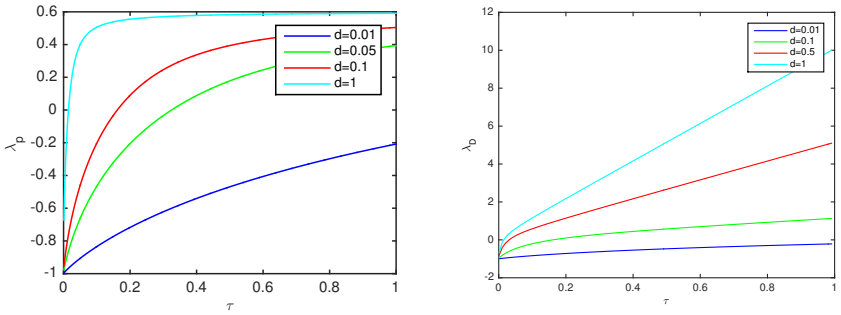

(a) (b)

Fig. 2 (a) λ_p versus τ (b) λ_D versus τ for $d = 0.01, 0.05, 0.1$ and 1 with $\delta = 0.15$

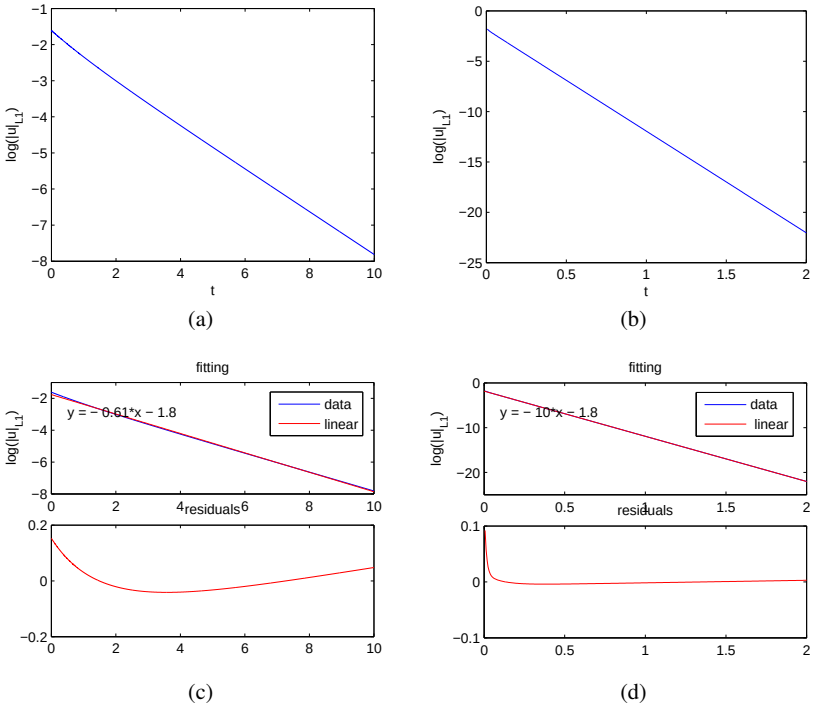

(a) (b) (c) (d)

Fig. 3 For large d, the population vanishes with exponential decay. In the above experiment, $d = 2$, $\tau = 0.5$, and timestep $= 0.4h^2$. 3(a) and 3(b) show the logarithm of the L_1 norm of u versus time. 3(c) and 3(d) are the linear fittings and the residues. The left column is for periodic boundary conditions and the right column is for Dirichlet boundary conditions.

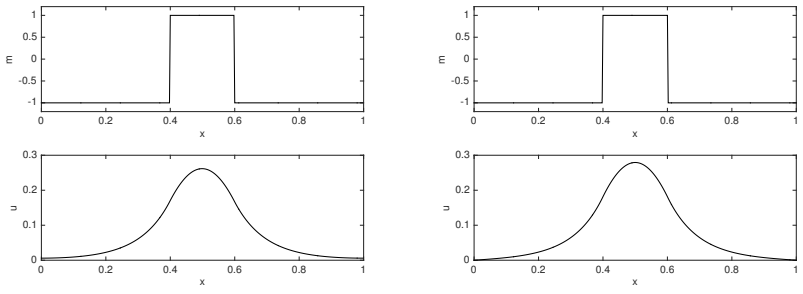

(a) (b)

Fig. 4 For small d, the population reaches a positive steady state eventually. Here, $d = 0.02$, $\tau = 0.5$, $\delta = 0.15$, $N = 400$, and timestep $= 0.4h^2$. 4(a) and 4(b) show the final configurations of u. The left column is for periodic boundary conditions and the right column is for Dirichlet boundary conditions.

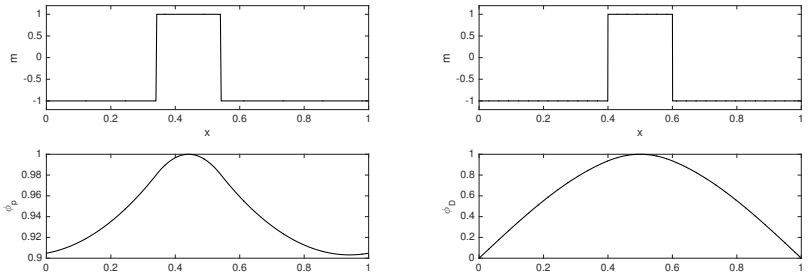

(a) (b)

Fig. 5 The optimal configuration of $m(x)$ and the corresponding eigenfunction computed by the rearrangement approach with $d = 0.8$, $\tau = 0.5$, $\delta = 0.15$ for (a) periodic boundary conditions ($\lambda_p = 0.57$) and (b) Dirichlet boundary conditions ($\lambda_D = 4.16$)

conditions, the optimal favorable region is connected, as shown in Fig. 5 with $d = 0.8$. Here our initial guess of $m(x)$ is

$$m(x) = \begin{cases} m_2 \text{ for } |x-0.4| < 0.05, |x-0.8| < 0.05 \\ m_1 \text{ for } \qquad\qquad \text{otherwise} \end{cases}$$

which has two positive intervals with a total area to be 0.2. For Dirichlet boundary conditions in Fig. 5(b), the optimal favorable region is found to be in the center of the domain with area 0.2, after 5 iterations. However, for periodic boundary conditions, the result is slightly different. For this particular initial m, after 3 iterations, the system reaches the optimization solution and the favorable region turns out as shown in Fig. 5(a), where the positive favorable region is still connected and with area 0.2, but in a different position. In fact, for periodic boundary conditions, the

positive favorable region does not necessarily stay fixed on one part of the domain in one dimensional case. The connected positive favorable region is transferable to any part of the domain, as long as it has the same total area. Thus, the numerical optimization solution depends on the initial guess of m. From the results of our numerical experiments, we see that the rearrangement algorithm converges in a few iterations.

4.2 Two-Dimensional Results

In two dimensions, we perform similar numerical tests as in one dimension with $m_1 = m_2 = 1$. On a square domain $[0,1] \times [0,1]$, we set the mesh size $Nx = Ny = 50$ for both periodic and Dirichlet boundary conditions. The initial guess of favorable region of $m(x)$ is a circle centered at $(0.5, 0.5)$ with radius 0.3. Using exactly the same parameters d and τ as in the one dimensional case, we plot in Fig. 6 (a) and (b) how the principal eigenvalue changes with respect to d for periodic and Dirichlet boundary conditions. In Fig. 7 we show the curves of λ_p and λ_D changing with respect to τ for different d. The results in two dimensions are very similar to the ones in one dimension. Both λ_p and λ_D gets smaller as d or τ decrease with the current choice of parameters.

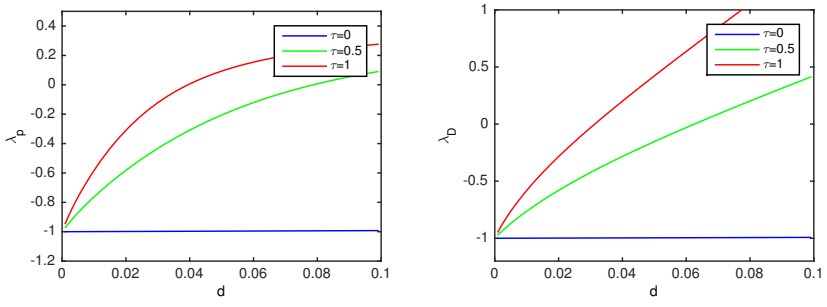

Fig. 6 (a) λ_p versus d (b) λ_D versus d with $\delta = 0.15$ for $\tau = 0, 0.5$, and 1 in the two dimensional case

In order to find the optimal favorable region in two dimensions, we solve the optimization problem using a rearrangement approach. First we study the problem on a square domain. We set the initial guess of $m(x)$ (Fig. 8) to be a cross centered at $(0.3, 0.3)$ with the definition below.

$$m(x,y) = \begin{cases} m_2 \text{ for } |x-0.3| < 0.1 \text{ and } |y-0.3| < 0.2, \\ m_2 \text{ for } |x-0.3| < 0.2 \text{ and } |y-0.3| < 0.1, \\ m_1 \text{ for } \quad \text{otherwise.} \end{cases} \tag{24}$$

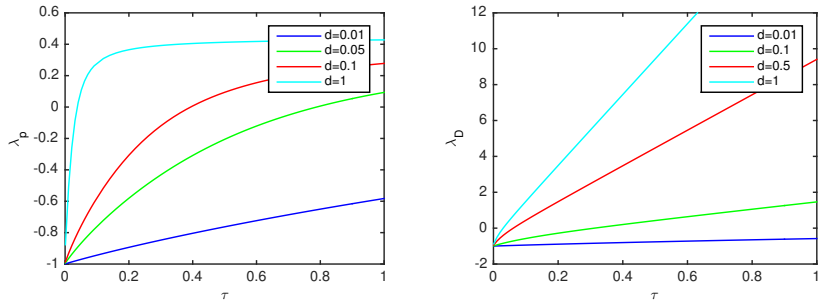

(a) (b)

Fig. 7 (a) λ_p versus τ (b) λ_D versus τ with $\delta = 0.15$ for $d = 0.01, 0.05, 0.1$, and 1 in the two dimensional case

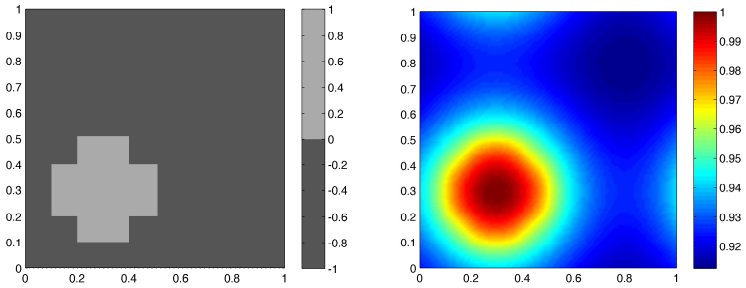

(a) m(x) (b) eigenfunction

Fig. 8 (a) Initial configuration of $m(x)$ with a cross shaped favorable region for the optimization problem and (b) its corresponding eigenfunction with periodic boundary conditions in two dimensions

The total area of the favorable region of the initial $m(x)$ is 0.12. For periodic boundary conditions, the optimized solution is reached after 3 iterations. In Fig. 9 we show the configuration of $m(x)$ and its corresponding eigenfunction at each iteration. As we can see, the optimal shape of the favorable region of m turns into a circular like shape during evolution.

Table 1 Values of λ_p and λ_D at each iteration during optimization procedure for $d = 1$, $\tau = 0.5$, $\delta = 0.15$, $N_x = N_y = 100$

Iteration	Periodic boundary	Dirichlet boundary
1	0.7398	10.499
2	0.7394	10.073
3	0.7394	10.070
4	0.7394	10.070

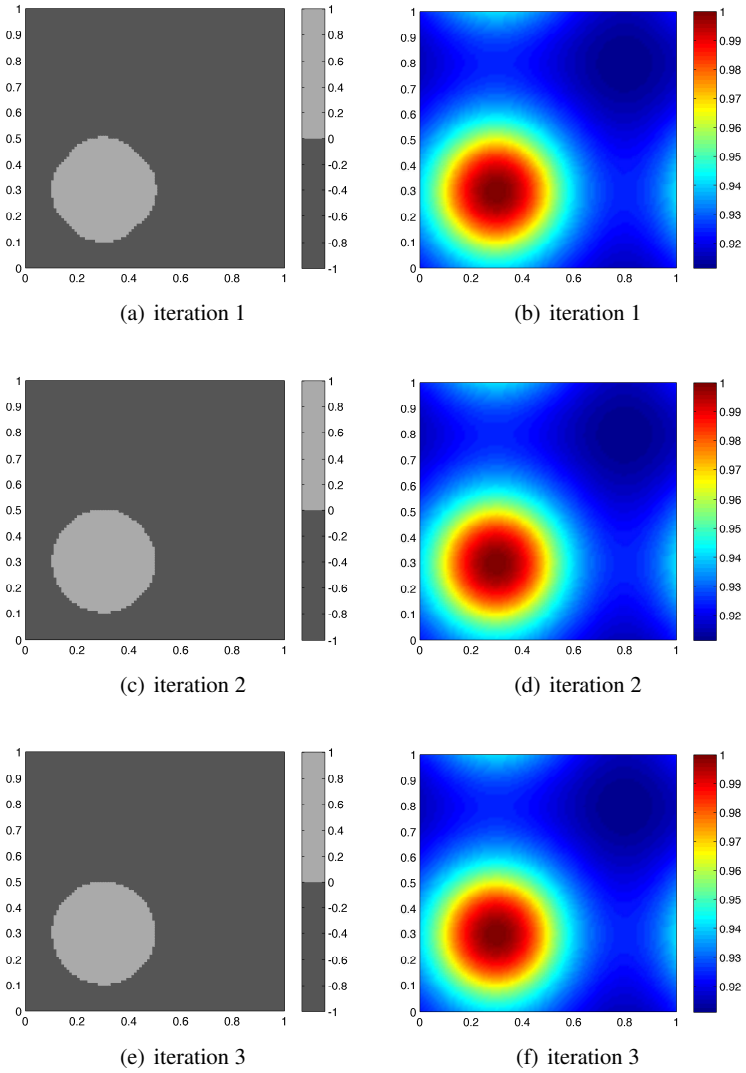

(a) iteration 1 (b) iteration 1

(c) iteration 2 (d) iteration 2

(e) iteration 3 (f) iteration 3

Fig. 9 The configuration of $m(x)$ and its corresponding eigenfunction for the first three numerical iterations. The optimal result $\lambda_p^* = 0.74$ is achieved at the 3rd iteration. The choice of parameters are $d = 1$, $\tau = 0.5$, $\delta = 0.15$, and $N_x = N_y = 100$.

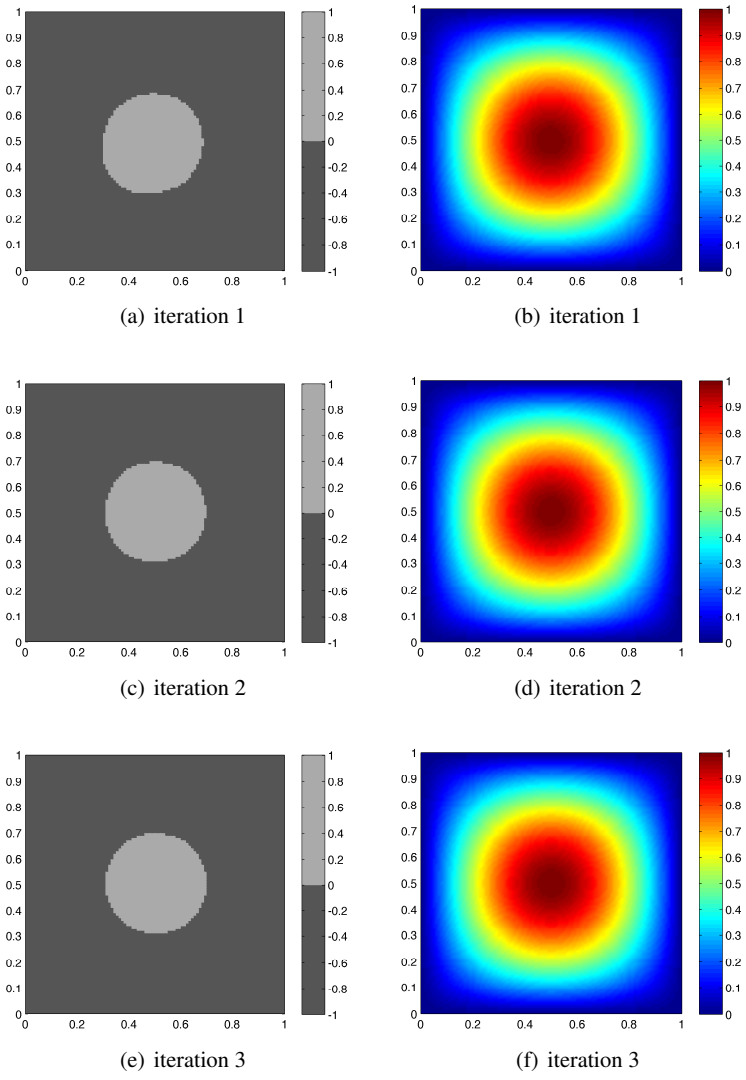

(a) iteration 1 (b) iteration 1

(c) iteration 2 (d) iteration 2

(e) iteration 3 (f) iteration 3

Fig. 10 The configuration of $m(x)$ and its corresponding eigenfunction for the first three numerical iterations. The optimal result $\lambda_D^* = 10.07$ is achieved at the 3rd iteration. The choice of parameters are $d = 1$, $\tau = 0.5$, $\delta = 0.15$, and $N_x = N_y = 100$.

For Dirichlet boundary conditions, the optimal result is also obtained after 3 iterations, as shown in Fig. 10. The favorable region again turns into a circular like shape but goes to the center of the domain, which is different from the periodic boundary case. As the number of iterations increases, λ_D decreases before settling at 10.07 in the end. In Table 1 , we show the values of λ_D for each iteration for both periodic and Dirichlet boundary conditions.

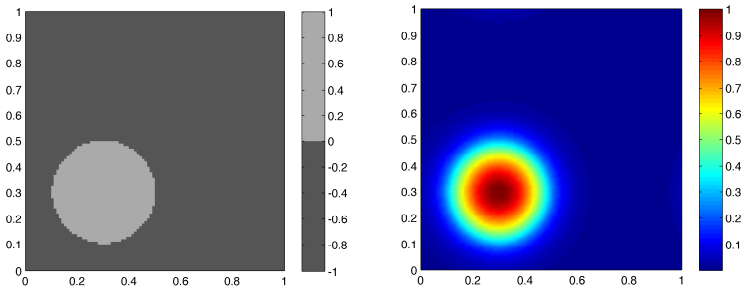

(a) iteration 4 (b) iteration 4

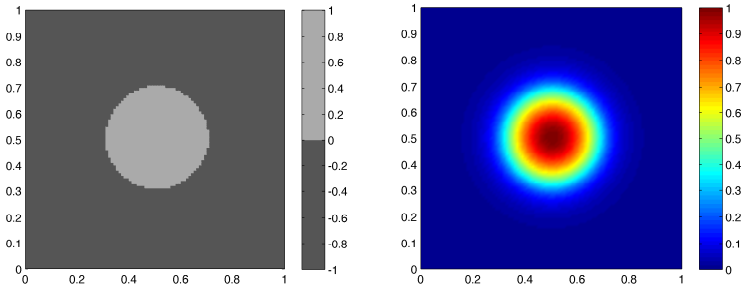

(c) iteration 4 (d) iteration 4

Fig. 11 The optimal configurations of $m(x)$ and their corresponding eigenfunctions at $4-$th numerical iteration for both periodic (top row) and Dirichlet boundary conditions (bottom row). The optimal eigenvalues are $\lambda_p^* = -0.54$ and $\lambda_D^* = -0.54$. The choice of parameters are $d = 0.01$, $\tau = 0.5$, $\delta = 0.15$, and $N_x = N_y = 100$.

In Fig. 11, we show the optimal results at 4-th iterations with negative eigenvalues when the choice of parameters are $d = 0.01$, $\tau = 0.5$, $\delta = 0.15$ for both periodic and boundary conditions. The initial guess for periodic boundary condition is (24) and the initial guess for Dirichlet boundary condition is (24) with the center of the cross shifted from $(0.3, 0.3)$ to $(0.5, 0.5)$. This choice of the initial condition gives the optimal configuration with fewer iterations. We observe that the results are similar to the optimal configuration with positive eigenvalues.

Next, we explore the results on rectangular domains with the same width, 1, but different heights, b. We set the initial guess of favorable region of m to be a square

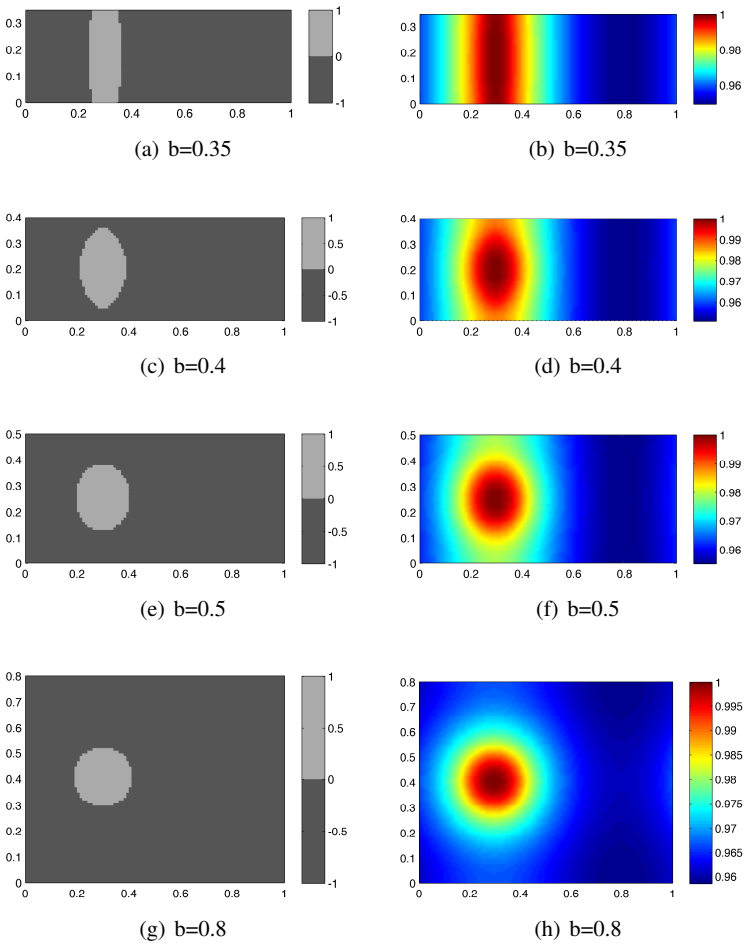

(a) b=0.35 (b) b=0.35

(c) b=0.4 (d) b=0.4

(e) b=0.5 (f) b=0.5

(g) b=0.8 (h) b=0.8

Fig. 12 The optimal favorable region and corresponding eigenfunction for $b = 0.35, 0.4, 0.5, 0.8$ for periodic boundary conditions. In these experiments, $d = 1$, $\tau = 0.5$, $\delta = 0.15$, $N_x = 100$, and $N_y = 100b$.

with width 0.2 centered at $(0.3, b/2)$. We calculate the optimal configurations of $m(x)$ for $b = 0.35$, 0.4, 0.5 and 0.8, for both periodic and Dirichlet boundary conditions, and present the final optimal m and the corresponding eigenfunctions in Fig. 12 for periodic boundary conditions and in Fig. 13 for Dirichlet boundary conditions. As we can see, for a periodic boundary, the optimal favorable region tends to a vertical band and touches the horizontal boundary for small b, and becomes a circular like shape when b turns bigger, which does not necessarily stay in the middle of the domain. However, for a Dirichlet boundary, for all choices of b examined,

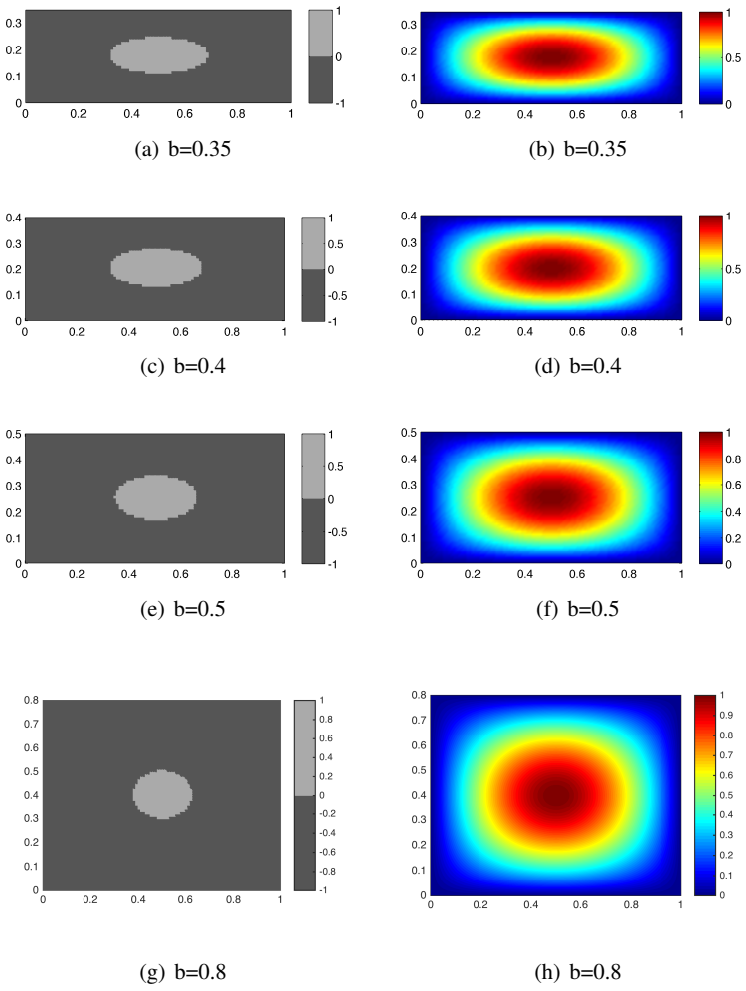

(a) b=0.35 (b) b=0.35

(c) b=0.4 (d) b=0.4

(e) b=0.5 (f) b=0.5

(g) b=0.8 (h) b=0.8

Fig. 13 The optimal favorable region and corresponding eigenfunction for $b = 0.35, 0.4, 0.5, 0.8$ for Dirichlet boundary conditions with $d = 1$, $\tau = 0.5$, $\delta = 0.15$, $N_x = 100$, and $N_y = 100b$

the positive resource tends to a circular like shape and moves to the center of the domain.

4.3 Dumbbell shaped domain

Here, we present numerical results via a finite element method on a dumbbell shaped domain with Dirichlet boundary conditions. The choice of parameters are $d = 1$,

$\tau = 0.5$, and $\delta = 0.15$. We are looking for an optimal configuration of the resource function $m(x)$ that minimizes the principal eigenvalue of (9). In the first experiment, the domain Ω is dumbbell shaped and the favorable region (corresponding to Ω_+) consists of two discs with the same radius located on both ends of the dumbbell. The initial and optimal (final) configurations of $m(x)$ with the eigenfunctions corresponding to the principal eigenvalue are shown in Fig. 14. The number of cells (quadrilaterals) in the domain is 25941. Table 2 shows the principal eigenvalue λ_D versus the iteration number.

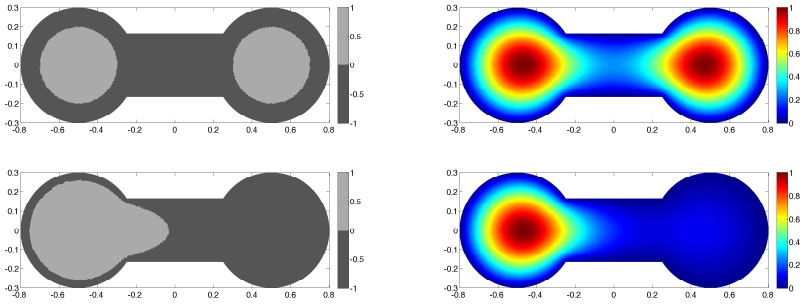

Fig. 14 Resource function $m(x)$ (left) and the eigenfunction $\phi_D(x)$ corresponding to the principal eigenvalue λ_D (right). The top row corresponds to the initial configuration and the bottom row corresponds to the optimal configuration after 9 iterations.

Table 2 The principal eigenvalue λ_D vs. iterations for a dumbbell shaped domain (see Fig. 14)

Iteration	0	2	4	6	8	10
λ_D	28.5249	28.4812	28.4797	28.4527	28.3513	28.3266

For the next experiment, the two discs for the initial favorable regions have different radii. Results of the computation in this case are shown in Fig. 15. Table 3 shows the principal eigenvalue λ_D after each iteration. As we see from the figures above, when the channel connecting the dumbbells is thinner, the optimal configuration of $m(x)$ is a single favorable region in either side. For cases where the two favorable regions on either side have different areas, the final configuration of $m(x)$ is concentrated on the side that had larger area initially. Next, we take a dumbbell shaped domain with a thicker channel. Initial favorable regions are again two discs located at both ends. Results of the case where the two discs have the same radius is shown in Fig. 16. The number of cells (quadrilaterals) in the domain is 21211. As we observe from the figure, the optimal favorable region is one large area in the middle of the thick channel away from the boundary. For the case when two discs that have different radii, we get a very similar configuration of $m(x)$.

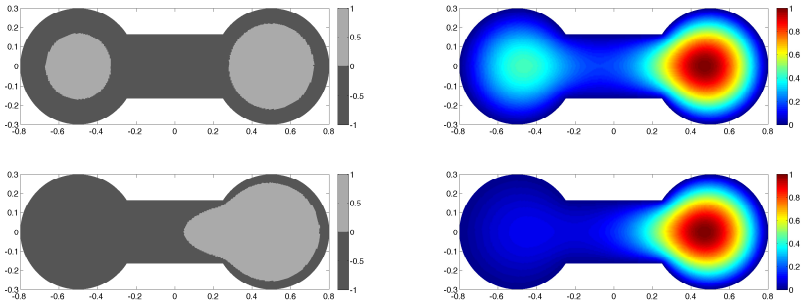

Fig. 15 Resource function $m(x)$ (left) and the eigenfunction $\phi_D(x)$ corresponding to the principal eigenvalue λ_D (right). The top row corresponds to the initial configuration and the bottom row corresponds to the optimal configuration after 3 iterations.

Table 3 The principal eigenvalue λ_D vs. iterations for a dumbbell shaped domain (see Fig. 15)

Iteration	0	1	2	3	4
λ_D	28.5123	28.3965	28.3416	28.3334	28.3334

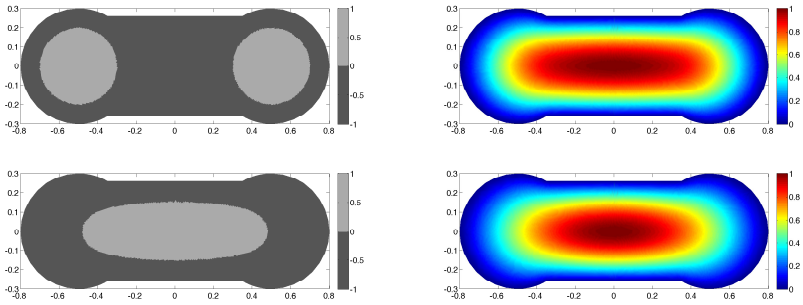

Fig. 16 Resource function $m(x)$ (left) and the eigenfunction $\phi_D(x)$ corresponding to the principal eigenvalue λ_D (right). The top row corresponds to the initial configuration and the bottom row corresponds to the optimal configuration after 4 iterations.

Table 4 The principal eigenvalue λ_D vs. iterations for a dumbbell shaped domain with thick channel (see Fig. 16)

Iteration	0	1	2	3	4	5
λ_D	20.0444	19.2431	19.2346	19.2346	19.2345	19.2345

5 Discussion

In this paper, we studied a mixed dispersal model with periodic and Dirichlet boundary conditions on different shapes of one-dimensional and two-dimensional domains both analytically and numerically. In terms of parameters values, we investigated two possible scenarios of longtime dynamics: the population of species dying off completely as time goes to infinity or converging to a non-trivial stationary distribution.

To analyze the convergence rate toward trivial and non-trivial stationary solutions, we estimated the principal eigenvalue of the corresponding linearized problem and solved the principal eigenvalue minimization problem in terms of the distribution of favorable and unfavorable regions. Our numerical simulations indicate that the optimal favorable region tends to be a simply-connected domain. Numerous results are shown to demonstrate various scenarios of optimal favorable regions for periodic and Dirichlet boundary conditions.

We would expect similar results for more general Robin-type boundary conditions. It would be interesting to analyze how the longtime dynamics can be affected by the application of spectral-parameter dependent boundary conditions (see [8] for example) or by replacing the linear diffusion term with non-linear diffusion, taking into account that the diffusion coefficient depends on population density. For example, the diffusion coefficient can be taken proportional to some positive or negative power of density, hence embracing the cases where the diffusion coefficient grows or decreases with the density which will lead eventually to interesting pattern formations [9].

As a future work we would also like to consider competition models when multiple species use different local and nonlocal dispersal strategies. Some results were already obtained in [23] on a model of two competing species.

Acknowledgements The authors would like to thank Institute for Mathematics and its Applications at University of Minnesota for hosting a special workshop on "WhAM! A Research Collaboration Workshop for Women in Applied Mathematics: Numerical Partial Differential Equations and Scientific Computing". This paper summarized the project results of Team3 on principal eigenvalue for a population dynamics model problem with both local and nonlocal dispersal.

Prepared by LLNL under Contract DE-AC52-07NA27344.

References

1. Bai, X., Li, F.: Optimization of species survival for logistic models with non-local dispersal. Nonlinear Analysis: Real World Applications **21**, 53–62 (2014)
2. Bai, X., Li, F.: Global dynamics of a competition model with nonlocal dispersal ii: The full system. Journal of Differential Equations **258**(8), 2655–2685 (2015)
3. Bangerth, W., Heister, T., Heltai, L., Kanschat, G., Kronbichler, M., Maier, M., Turcksin, B., Young, T.D.: The `deal.II` library, version 8.2. Archive of Numerical Software **3** (2015)
4. Cantrell, R.S., Cosner, C.: Diffusive logistic equations with indefinite weights: population models in disrupted environments. Proceedings of the Royal Society of Edinburgh: Section A Mathematics **112**(3-4), 293–318 (1989)

5. Cantrell, R.S., Cosner, C.: Diffusive logistic equations with indefinite weights: population models in disrupted environments ii. SIAM Journal on Mathematical Analysis **22**(4), 1043–1064 (1991)
6. Cantrell, R.S., Cosner, C.: Spatial ecology via reaction-diffusion equations. John Wiley & Sons (2004)
7. Chasseigne, E., Chaves, M., Rossi, J.D.: Asymptotic behavior for nonlocal diffusion equations. Journal de mathématiques pures et appliquées **86**(3), 271–291 (2006)
8. Chugunova, M.: Inverse spectral problem for the sturm-liouville operator with eigenvalue parameter dependent boundary conditions. In: Operator theory, system theory and related topics, pp. 187–194. Springer (2001)
9. Colombo, E.H., Anteneodo, C.: Nonlinear diffusion effects on biological population spatial patterns. Physical Review E **86**(3), 036,215 (2012)
10. Cortazar, C., Coville, J., Elgueta, M., Martinez, S.: A nonlocal inhomogeneous dispersal process. Journal of Differential Equations **241**(2), 332–358 (2007)
11. Cortázar, C., Elgueta, M., García-Melián, J., Martínez, S.: Existence and asymptotic behavior of solutions to some inhomogeneous nonlocal diffusion problems. SIAM Journal on Mathematical Analysis **41**(5), 2136–2164 (2009)
12. Cosner, C., Dávila, J., Martínez, S.: Evolutionary stability of ideal free nonlocal dispersal. Journal of Biological Dynamics **6**(2), 395–405 (2012)
13. Coville, J.: On a simple criterion for the existence of a principal eigenfunction of some nonlocal operators. Journal of Differential Equations **249**(11), 2921–2953 (2010)
14. Coville, J., Dávila, J., Martínez, S.: Existence and uniqueness of solutions to a nonlocal equation with monostable nonlinearity. SIAM Journal on Mathematical Analysis **39**(5), 1693–1709 (2008)
15. Coville, J., Dávila, J., Martínez, S.: Nonlocal anisotropic dispersal with monostable nonlinearity. Journal of Differential Equations **244**(12), 3080–3118 (2008)
16. Coville, J., Davila, J., Martinez, S.: Pulsating fronts for nonlocal dispersion and kpp nonlinearity. Annales de l'Institut Henri Poincare (C) Non Linear Analysis **30**(2), 179–223 (2013)
17. Coville, J., Dupaigne, L.: On a non-local equation arising in population dynamics. Proceedings of the Royal Society of Edinburgh: Section A Mathematics **137**(04), 727–755 (2007)
18. Deng, K.: On a nonlocal reaction-diffusion population model. Discrete and Continuous Dynamical Systems Series B **9**(1), 65 (2008)
19. Henrot, A.: Extremum problems for eigenvalues of elliptic operators. Springer Science & Business Media (2006)
20. Hintermüller, M., Kao, C.Y., Laurain, A.: Principal eigenvalue minimization for an elliptic problem with indefinite weight and robin boundary conditions. Applied Mathematics and Optimization **65**(1), 111–146 (2012)
21. Jin, Y., Lewis, M.A.: Seasonal influences on population spread and persistence in streams: critical domain size. SIAM Journal on Applied Mathematics **71**(4), 1241–1262 (2011)
22. Jin, Y., Lewis, M.A.: Seasonal influences on population spread and persistence in streams: spreading speeds. Journal of Mathematical Biology **65**(3), 403–439 (2012)
23. Kao, C.Y., Lou, Y., Shen, W.: Random dispersal vs. nonlocal dispersal. Discrete and Continuous Dynamical Systems **26**(2), 551–596 (2010)
24. Kao, C.Y., Lou, Y., Shen, W.: Evolution of mixed dispersal in periodic environments. Discrete and Continuous Dynamical Systems B **17**(6), 2047–2072 (2012)
25. Kao, C.Y., Lou, Y., Yanagida, E.: Principal eigenvalue for an elliptic problem with indefinite weight on cylindrical domains. Mathematical Biosciences and Engineering **5**(2), 315–335 (2008)
26. Kao, C.Y., Su, S.: Efficient rearrangement algorithms for shape optimization on elliptic eigenvalue problems. Journal of Scientific Computing **54**(2-3), 492–512 (2013)
27. Li, F., Lou, Y., Wang, Y.: Global dynamics of a competition model with non-local dispersal i: The shadow system. Journal of Mathematical Analysis and Applications **412**(1), 485–497 (2014)
28. Lutscher, F.: Nonlocal dispersal and averaging in heterogeneous landscapes. Applicable Analysis **89**(7), 1091–1108 (2010)

29. Shen, W., Xie, X.: On principal spectrum points/principal eigenvalues of nonlocal dispersal operators and applications. arXiv preprint arXiv:1309.4753 (2013)
30. Skellam, J.: Random dispersal in theoretical populations. Biometrika pp. 196–218 (1951)
31. Sun, J.W.: Existence and uniqueness of positive solutions for a nonlocal dispersal population model. Electronic Journal of Differential Equations **2014**(143), 1–9 (2014)
32. Volpert, V., Vougalter, V.: Existence of stationary pulses for nonlocal reaction-diffusion equations. Documenta Mathematica **19**, 1141–1153 (2014)